Catalysis Today 147 (2009) 211–216

Contents lists available at ScienceDirect

Catalysis Today

journal homepage: www.elsevier.com/locate/cattod

Crystalline order of silver–gold nanocatalysts with hollow-core and alloyed-shell

Domingo A. Ferrer [a], Luis A. Diaz-Torres [a], Shaomin Wu [a], Miguel Jose-Yacaman [a,b,*]

[a] Materials Science and Engineering Program, Texas Materials Institute, The University of Texas at Austin, Austin, TX, United States
[b] Department of Physics and Astronomy, The University of Texas at San Antonio, San Antonio, TX, United States

ARTICLE INFO

Article history:
Available online 17 April 2009

Keywords:
Bimetallic nanoparticles
Transmission electron microscopy
Gold
Silver
Weak-beam dark field

ABSTRACT

This paper reports the internal structure of Ag–Au bimetallic nanoparticles with hollow interiors and alloyed shells, synthesized by chemical reduction of metallic precursor and subsequent galvanic replacement reaction. By taking advantage of advanced electron microscopy methods such as high-resolution transmission electron microscopy (HRTEM), scanning TEM (STEM), weak beam dark-field (WBDF) microscopy, X-ray energy dispersive spectroscopy (EDS) and nano-beam electron diffraction (NBD), sufficient and necessary evidences confirm the sacrificial role of silver nanoparticles as templates for the epitaxial deposition of gold-rich atomic layers.

1. Introduction

Bimetallic nanoparticles, where two different metal elements exist in one particle, have interesting catalytic, electronic, and optical properties distinct from those of the corresponding monometallic counterparts [1–6]. The properties of bimetallic nanoparticles can vary significantly with their size and shape, as happens in monometallic nanoparticles, and with the structure and the chemical composition as well. Due to this correlation, control of morphology and composition for bimetallic nanoparticles is important for the development of novel cluster-assembled nanomaterials [3,5]. Alloyed and layered nanoclusters are the two major forms of bimetallic nanoparticles. In many cases layered bimetallic nanoclusters display a core–shell structure, where a thin shell of metal surrounds a core of a different metal. Recently, three-layer (Pd@Au@Pd) [4] and four-layer (Ag@Au@Ag@Ag) [10] core–shell structures were also reported in gold–palladium and gold–silver systems respectively. Here we report another form of bimetallic nanoparticles: Ag–Au nanoparticles with hollow cores and alloyed shells.

Au and Ag bimetallic systems have received enormous attention not only because of their chemical stability, but also due to their unique properties in catalysis, SERS and biomedical applications [5–10]. In spite of the well-known inertness of gold, when finely dispersed it reveals extraordinary catalytic activity for the epoxidation of propene and the oxidation of CO [11–13]. Gold-based catalysts display attractive applications in automotive emission control, owing to they stay active at low temperatures (room temperature) unlike platinum or palladium catalysts [12]. Nanoporous gold, showing a spongelike morphology, obtained through selective leaching of silver from gold–silver alloys has surprisingly high catalytic activity for CO oxidation at ambient pressures and temperatures as low as 0 °C [11]. On the other hand, sintered compacts can impede the catalytic applications of gold-based materials.

Nanoporous gold possesses good thermal stability and excellent reproducibility. Most importantly, the curved shape of its ligaments includes a high density of low-coordinate surface sites, such as step and kink atoms of great importance in catalysis [13,14]. In addition to this, it has been discussed that Ag residues at the surface of the nanoporous foam are also involved in the catalytic cycle [15]. Moreover, while pure gold already shows high catalytic activity, silver content can significantly enhance the performance of the Au-based catalysts [11–13].

Ag–Au alloy nanoparticles of certain bimetallic compositions can be synthesized when salts of both metals are simultaneously reduced [5–8]. Core–shell Ag–Au colloids were generated via successive reduction of the different metal salts have also been studied [9,10]. Hollow nanostructures prepared by various synthesis methods have been reported in almost every material system. Metallic nanostructures with hollow interiors such as gold nanoshells and gold nanocages were synthesized by galvanic replacement reaction between Ag templates and aqueous $HAuCl_4$ by Xia and coworkers [16–18]. Yin et al. [19] observed the formation of cobalt-rich hollow nanocrystals through a mechanism analogous to the Kirkendall Effect [19]. Fabrication of polymeric hollow nanostructures using silver bromide as tem-

* Corresponding author at: Department of Physics and Astronomy, The University of Texas at San Antonio, San Antonio, TX, United States.
E-mail address: miguel.yacaman@utsa.edu (M. Jose-Yacaman).

0920-5861/$ – see front matter © 2009 Published by Elsevier B.V.
doi:10.1016/j.cattod.2009.02.047

plates were also reported [20]. However, most of the authors claimed hollow nanostructures only by showing a contrast difference of darker shell and brighter core in bright field TEM images. The contrast in bright field TEM images is determined by many factors such as mass-thickness and Z-number. Moreover, the conclusions on whether the composition of the shells of hollow cubes prepared by Xia and coworkers [17] was pure Au or Au/Ag alloy were controversial. Therefore, only bright field TEM does not provide enough experimental evidence to judge the composition and detailed structure of void nanocrystals. Further analyses are needed to completely characterize the nanostructures.

In this paper, we present the synthesis and the characterizations of Ag–Au bimetallic nanoparticles with alloyed shells and hollow cores. Our fabrication approach involves chemical reduction of metal salt and galvanic replacement reaction between Ag atoms and $AuCl_4^-$ ions. High-resolution transmission electron microscopy (HRTEM), scanning TEM (STEM), weak beam dark-field (WBDF) microscopy, nano-beam electron diffraction (NBD) and X-ray energy dispersive spectroscopy (EDS) were employed to study the chemical composition and the detailed structure of the nanoparticles. More convincing conclusions can be drawn on those hollow nanoparticles with different shapes according to the complete microanalysis results.

2. Experimental

The Ag–Au hollow nanoparticles were prepared by first synthesizing the Ag colloid and then carrying out a galvanic replacement reaction between as-synthesized Ag nanoclusters and $AuCl_4^-$ ions. Similar to Lee and Meisel method [21], 4 mL of a 1% (w/v) sodium citrate solution was added to 200 mL of 1 mM $AgNO_3$ solution, with deionized (DI) water as solvent in both solutions. Then the mixture was heated up and kept boiling for 1 h. The color of the solution turned to greenish yellow indicating the formation of Ag nanoparticles. Based on the galvanic replacement process described by Xia and coworkers [18], 1 mL of 0.3 mM aqueous solution of $HAuCl_4$ was added to 5 mL of as-synthesized Ag colloid drop-by-drop with continuous stirring. A color change from greenish yellow to brown and finally dark blue was observed while $HAuCl_4$ was being added. TEM grids were prepared by dropping the samples on copper grids with carbon support film. A JEOL 2010F transmission electron microscope equipped with ultra-high resolution pole piece (C_s = 0.5 mm) and Gatan 2D digital-parallel acquisition software was used to record high-resolution bright field TEM images, WBDF images, NBD patterns for the nanoparticles. The microscope was employed under Scherzer defocus condition [22], which occurs at

$$\Delta f_{Sch} = -1.2(Cs\lambda)^{1/2} \quad (1)$$

to assure the best interpretable resolution, where Δf_{Sch} corresponds to the defocus value, C_s defines the spherical aberration coefficient and λ is the wavelength determined by the accelerating voltage.

Nano-beam electron diffraction patterns were obtained with a probe size of 1.5 nm to study a specific area in an individual nanoparticle by means of a JEOL TEM 2010-F. STEM pictures and STEM-EDS line scanning results were acquired using a FEI Tecnai TF20 field-emission transmission electron microscope. The acceleration voltage for both microscopes was 200 kV.

3. Results and discussions

The core–shell pattern can be clearly recognized for the Ag–Au nanoparticles both in TEM bright field and STEM images displayed in Fig. 1a and b respectively. Since both mass-thickness and Z-number contribute to the contrast, bright shells and dark cores can indicate plate-like nanostructures with the periphery thicker than the center, nanoparticles with hollow interiors, or Ag–Au core–shell nanoclusters and so on. The samples were observed at different tilting angles. No change in shape and contrast was found, thus eliminating the possibility of plate-like nanostructures.

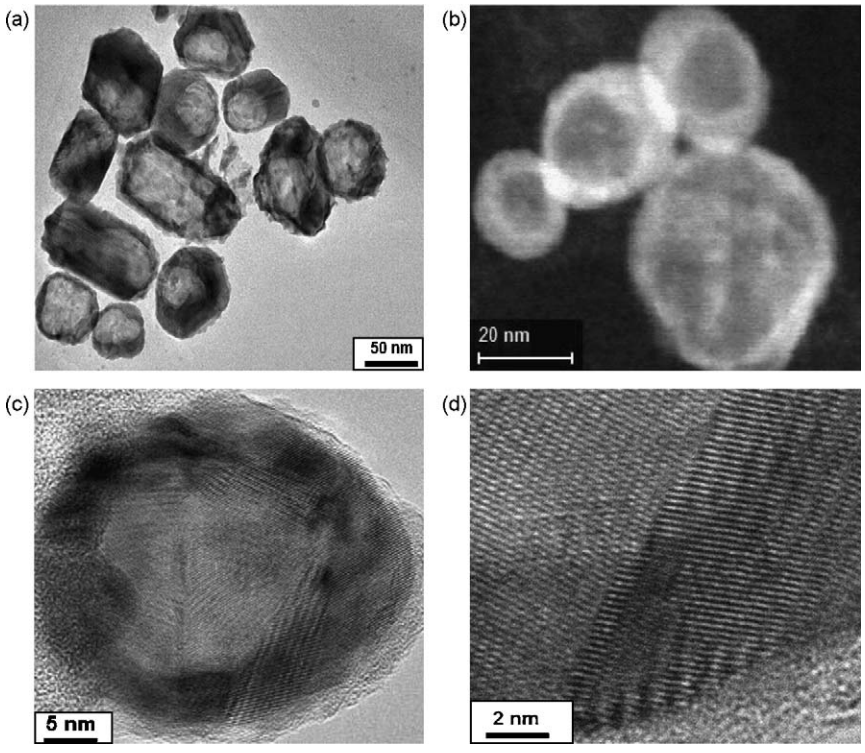

Fig. 1. (a) TEM (b) STEM image of the Ag–Au nanoparticles with Ag/Au alloy shells and hollow cores. (c, d) High-resolution TEM images of an individual Ag–Au nanoparticle.

Images acquired under high HRTEM (Fig. 1c and d) revealed that core and shell have a different crystal orientation. This evidences the formation of the gold shell on the silver seeds. HRTEM and STEM Images of the original silver seeds are shown as supplementary information.

The size distribution of the nanoparticles was determined for the Ag seeds, and showed a mean diameter and polydispersity of 53.6 ± 9.1 nm (supplementary information). Once the $HAuCl_4^-$ species were mixed with the silver nanocrystals for 30 min, the size of the nanoparticles changed to 68.2 ± 11.2 nm (Fig. 1a and b). The dimensions of the nanoparticles exhibited a slight increase in the outer diameter caused by the deposition of gold atoms on the surface of the silver seeds.

Energy dispersive spectroscopy analysis under bright field TEM mode on a single nanoparticle revealed that the atomic percentage of Au in a typical Ag–Au nanoparticle is about 13%. According to the stoichiometry [18]

$$3Ag_{(s)} + AuCl_4^- \rightarrow Au_{(s)} + 3Ag^+ + 4Cl^- \quad (2)$$

in the galvanic replacement reaction the ratio of the $AuCl_4^-$ ions with respect to the Ag atom is roughly 10%. This is consistent with the experiment conditions calculated based on the molar concentration of the solutions. Since the lattice constants of Ag and Au are extremely similar (4.078 Å for Au and 4.086 Å for Ag), a 13% atomic percentage of Au in a Ag–Au nanoparticle would result in a shell with a thickness of only 1/20th of the radius of a spherical particle, if the shell consisted of pure Au. Therefore the outer shell of the nanoparticle with a thickness shown in Fig. 1 must be Ag/Au alloy.

The galvanic replacement reaction described here is driven by an electroless mechanism, involving spontaneous reduction of metal ions to metallic particles and films in the absence of external sources of electric current. This heterogeneous process is frequently employed for preparing metallic nanostructures by consuming the more reactive component. Since the standard reduction potential of $AuCl_4^-$/Au pair (0.99 V vs standard hydrogen electrode, SHE) is larger than that of the Ag^+/Ag pair (0.80 V vs SHE) [16], solid silver is oxidized into Ag^+ when silver nanocrystals and $HAuCl_4$ are blended in an aqueous medium. The temperature of the reaction does not seem to play a fundamental role in this process.

The surface of silver nanoparticle seeds serve as reducing agent and electron source for reduction of the $AuCl_4^-$ supplied by the metallic salt ($HAuCl_4$). The shell deposition can continue as long as silver ions can permeate and electrons can transfer through the shell. This seed-mediated mechanism might not be affected by the oxygen content of the aqueous medium.

EDS line scanning across the whole nanostructure in the STEM mode was carried out to analyze the distribution of the chemical composition (Fig. 2a and b). When scanning the peripheral region of the Ag–Au nanoparticle, both Au and Ag peaks appear in the spectrum shown in Fig. 2(b), likely indicating Ag/Au alloying again. The X-ray signal intensity drops to minimum in the central region, although does not completely disappear as shown in Fig. 2(a). This is due to the three-dimensional shape of the nanoparticle. Photons generated in the shell also contribute to the total signal when scanning the central area. Weak signals from the core which are also indicated by a dip in the total EDS signal counts in Fig. 2 suggest a hollow or porous core. Elemental line profiling is another powerful feature that EDS-STEM analysis provides. Fig. 2(c) gives the Ag and Au single element composition profile across the nanostructure. The minimum Ag signal in the center supports the previous argument of a hollow or porous core, because the Ag/Au alloy shell with a solid pure Ag core should have Ag signal peaked in the center. The evenly distributed Au signals are present all over

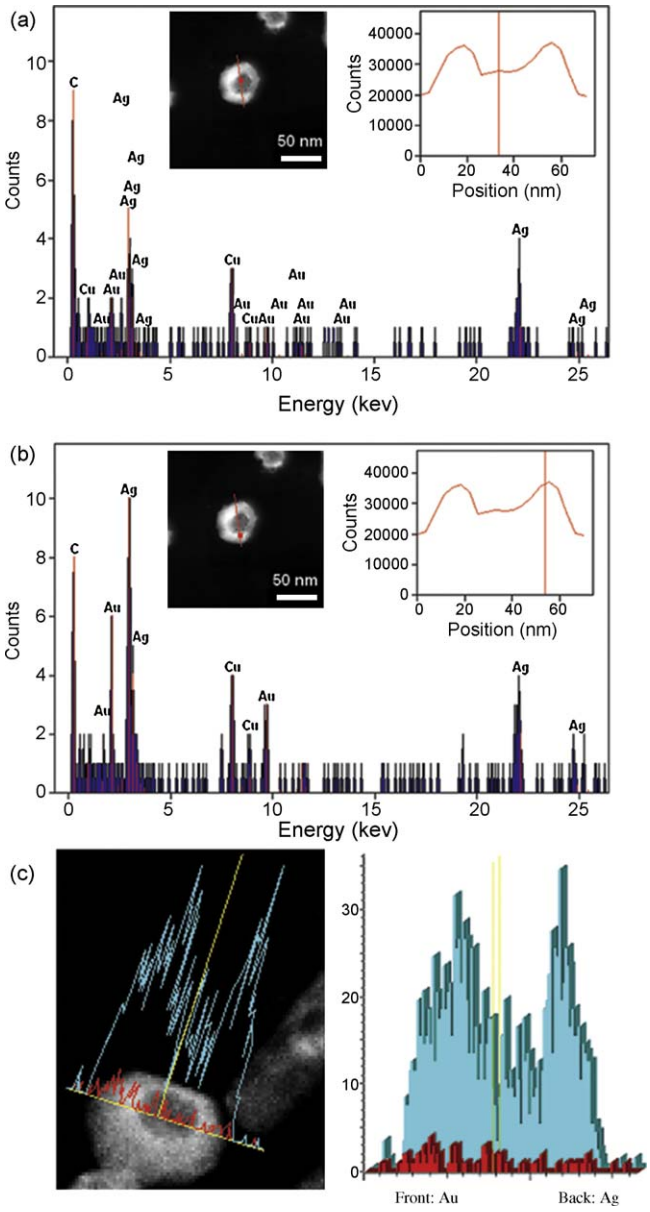

Fig. 2. STEM-EDS line scanning analysis: EDS signals from the central (a), and peripheral (b) regions. (c) Ag and Au composition profile on an individual Ag–Au nanoparticle.

the analyzed shell. For typical Ag–Au nanoparticles, the Ag/Au ratios obtained from the EDS signal are equal between the peripheral and central region, confirming the Ag–Au bimetallic nanoparticles with alloyed shells and completely hollow cores. For larger nanoparticles, the Ag/Au ratio is higher in the center, implying that pure Ag still exists in the core and very likely it is porous. The result did not change when the samples were tilted at different angles along either axis.

The WBDF method is often used for illustrating the thickness change and morphology of nanoparticles by tilting the sample or the electron beam away from the Bragg's condition [23]. Under the exact Bragg's condition, a single crystal nanoparticle shows uniform contrast while multiple-twinned particles (MTP) and polycrystalline nanoparticles do not. Fig. 3 shows the WBDF image of a typical Ag–Au nanoparticle with hollow core at Bragg's condition. The large contrast variation over the whole nanoparticle suggests that the crystal orientation changes at different areas of the nanostructure.

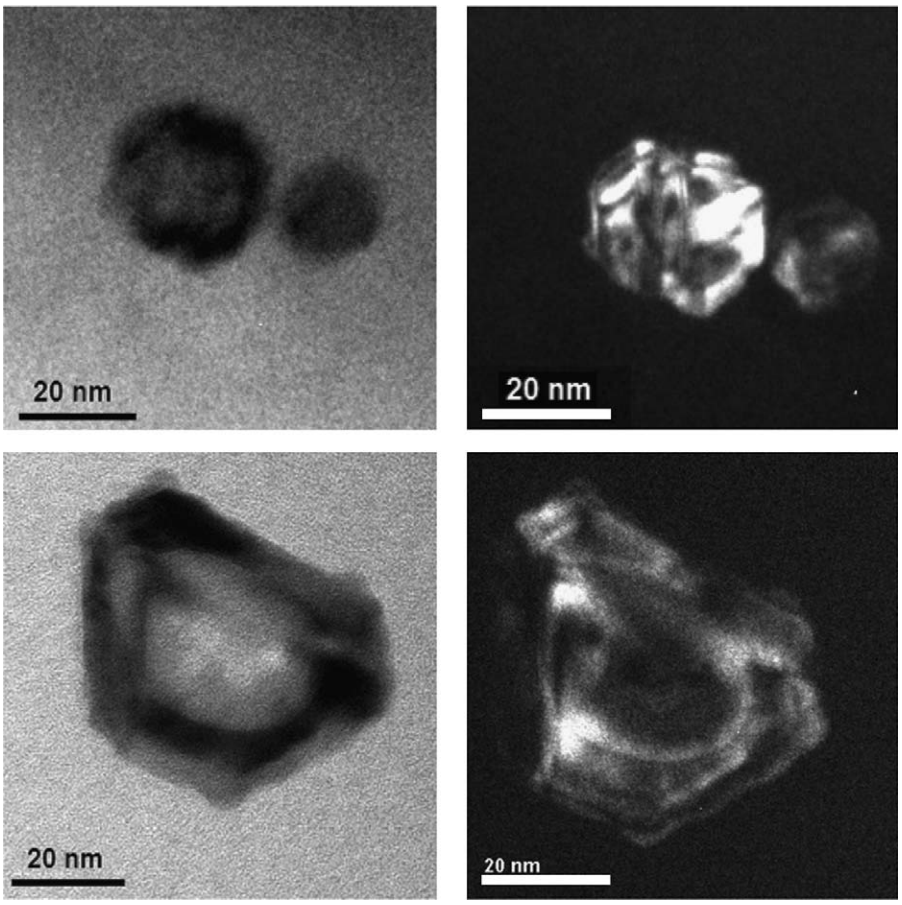

Fig. 3. TEM (left) and WBDF bright field (right) images of Ag–Au nanoparticles with hollow cores.

Nano-beam electron diffraction (NBD) allows us to investigate the crystal structure in an area down to nanoscale by using a concentrated while still nearly parallel electron beam with the probe size as small as a few nanometers or less. The indexed NBD patterns obtained from different parts of two typical Au–Ag hollow nanoparticles with a probe size of 1.5 nm are displayed in Fig. 4. The diffraction patterns varied with the probe position on the Ag–Au hollow nanoparticle #1 verifying our inference on the crystal orientation change from WBDF images. Some diffraction spots split into doublets on Fig. 4(a) indicating micro twinning in the nanoparticle. The twinning can also be observed on the high-resolution bright field TEM image of Fig. 1(c). The extra diffraction spots shown on the NBD pattern of Ag–Au hollow nanoparticle #2 are contributed by the lattice planes whose reflections are not supposed to appear. We believe that this is because there is more than one grain in the area that the electron beam probed. The extra spots must be from another neighboring grain in the area.

A sketch proposing the major steps implicated in the galvanic replacement process is depicted in Fig. 5. After the $HAuCl_4$ solution has been mixed with the dispersion of silver nanoparticles, the replacement reaction will start from the sites with relatively high surface energies, which typically include steps, point defects, and stacking faults. Once the reaction has begun on the active site of each seed, the silver would start dissolving and a hole would be generated on the facets (anode reaction). This reaction resembles a corrosion process, with silver being oxidized at the anode. The released electrons can easily migrate to the surface of the nanoparticle, available to reduce $AuCl_4^-$ into Au atoms (cathode reaction).

The elemental gold formed during the galvanic replacement reaction preferentially deposits on the surface of each seed owing to a good matching among the crystalline structures [16,17]. Gold and silver are face-centered cubic and display close lattice constants as mentioned before. The epitaxial deposition of the alloyed shell guides the formation of a thin, incomplete layer of gold (Fig. 5, step a), which can avoid the underside silver from reacting with $HAuCl_4$. As a consequence, the hole will continue to act as an active site for subsequent reaction. Simultaneously, this opening on the surface enables all the species (e.g., $AuCl_4^-$, Ag^+, Cl^-, and Au^+) to incessantly diffuse inwards and outwards the hole. The dissociated silver transforms each seed into a shallow interior structure (Fig. 5, step b). The generated gold atoms continue depositing on the outer surface of the silver template and gradually diminish the area of opening by distinct mass diffusion processes. As the reaction proceeds, the internal void will expand to maximum size with relatively uniform and homogeneous walls (Fig. 5, step c).

The galvanic replacement reaction between the silver seed and $HAuCl_4$ (Fig. 5, steps a, b, and c) involves alloying events due to the diffusion rates of silver and gold atoms are considerably high at room temperature. In fact, silver and gold form a solid solution owing to the homogeneous Au–Ag alloy display higher stability than either pure Au or Ag [24]. The occurrence of lattice vacancies can be also explained as consequence of the substitution of one gold atom at the expense of three silver atoms, according to the stoichiometric expression shown in Eq. (2). These structural defects can generate concave morphologies for the solid walls, and thus cause the interfacial area and the surface energy to increase. Q1

The optical absorption spectrum of pure Ag nanoparticles and Ag–Au bimetallic nanoparticles with three different Au concentrations was collected using a Cary 5000 UV–vis NIR Spectrometer, as shown in Fig. 6. The pure Ag nanoparticles solution has a

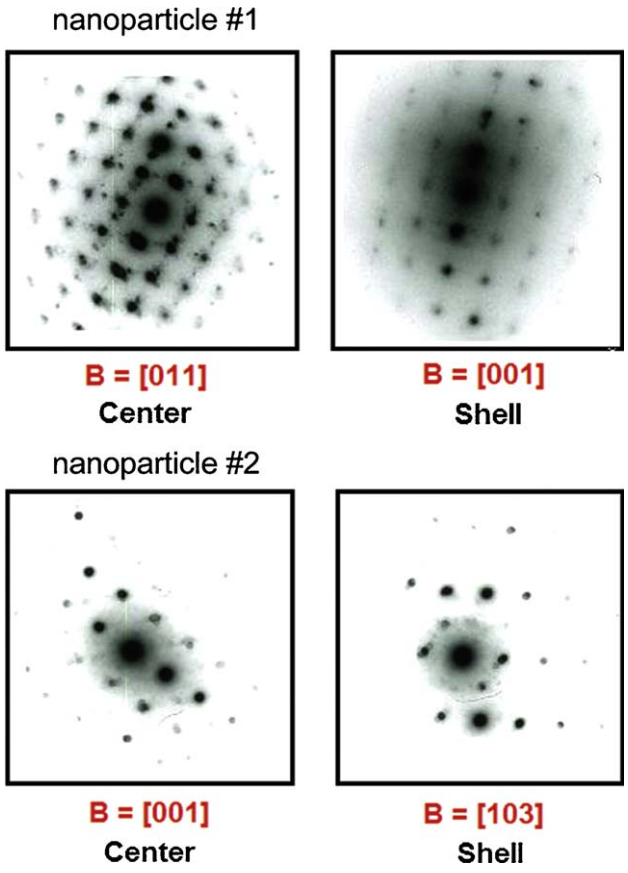

Fig. 4. Electron diffraction patterns of two different Ag–Au nanoparticles in the core and shell regions.

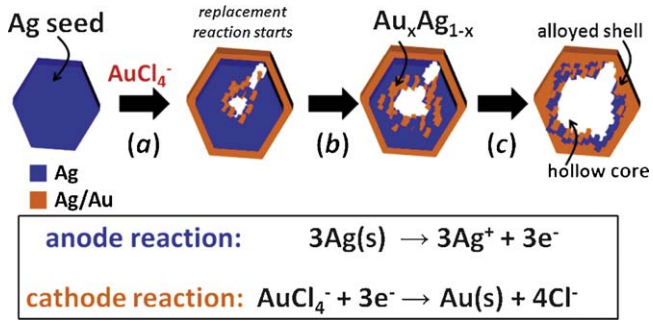

Fig. 5. Proposed mechanism for the formation of Ag–Au nanoparticles with *hollow-core alloyed-shell* morphology.

characteristic resonance peak at 410 nm, similar to the signal detected in previous reports [5–7]. The absorption peak of the Ag–Au hollow nanoparticles described above is at 590 nm. Compared to the pure Au solid nanoparticles which have a peak wavelength of 520 nm, the peak of the Ag–Au hollow nanoparticles is red shifted by 70 nm. This difference can be attributed to the hollow core morphology of the nanocrystals after the effect of the galvanic replacement reaction. The spectra of the Ag–Au nanoparticles with half and twice of the Au concentration of the Ag–Au hollow nanoparticles are also displayed in Fig. 6. The broadening of the spectrum peak with higher Au concentration is due to the increase of the variation of Au concentration in the Ag–Au nanoparticles when more Au ions were added during the galvanic replacement reaction.

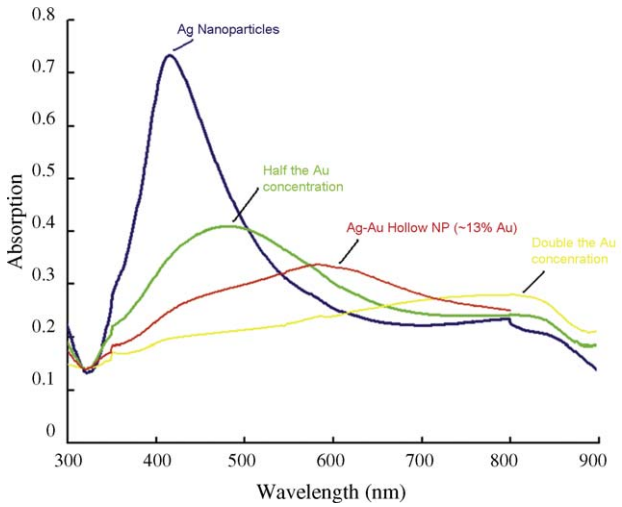

Fig. 6. UV–vis spectrum of Ag–Au nanoparticles with different Au concentration.

4. Conclusions

Sufficient and necessary analyses have been performed using TEM and related techniques on the Ag–Au bimetallic nanoparticles to determine their detailed structure, composition distribution and crystalline properties. The nanoparticles are typically spherical, polycrystalline, consisting of Ag/Au alloyed shells and hollow cores. The surface plasmon resonance peak of Ag–Au hollow nanostructures have a substantial red shift comparing to that of solid Ag–Au bimetallic nanoparticles. The method described above can be generally applied to the characterization of most of the hollow nanostructures with large Z-number materials present. For low Z-number material system, Electron Energy Loss Spectroscopy (EELS) may be more suitable than EDS line scanning. We have studied the selective removal of Ag atoms and the concurrent deposition of Au in the dealloying process. The detailed TEM analysis of these nanostructures with hollow interiors allows us to monitor how silver nanoparticles evolve from solid objects into core/shell hollow nanoparticles.

Acknowledgments

The authors thank the Center for Nano and Molecular Science and Technology, the Texas Materials Institute, and the International Center for Nanotechnology and Advanced Materials in The University of Texas at Austin. We also thank the support from the Welch Foundation and the NSF Grant DMR-0602587: "Alloys at the Nanoscale: The case of Nanoparticles".

Appendix A. Supplementary data

Supplementary data associated with this article can be found, in the online version, at doi:10.1016/j.cattod.2009.02.047.

References

[1] Y.H. Chen, U.J. Nickel, Chem. Soc. Faraday Trans. 89 (1993) 2479.
[2] J. Turkevich, G. Kim, Science (1970) 873.
[3] D.I. Garcia-Gutierrez, C.E. Gutierrez-Wing, L. Giovanetti, J.M. Ramallo-Lopez, F.G. Requejo, M. Jose-Yacaman, Phys. Chem. B (2005) 3813.
[4] D. Ferrer, A. Torres-Castro, X. Gao, S. Sepulveda-Guzman, U. Ortiz-Mendez, M. Jose-Yacaman, Nano Lett. 7 (2007) 1701.
[5] N.N. Kariuki, J. Luo, M. Maye, S.A. Hassan, T. Menard, H.R. Naslund, Y. Lin, C. Wang, M.H. Engelhard, C.-J. Zhong, Langmuir 20 (2004) 11240.
[6] L. Rivas, S. Sanchez-Cortes, J.V. Garcia-Ramos, G. Morcillo, Langmuir 16 (2000) 9722.
[7] A.V. Singh, B.M. Bandgar, M. Kasture, B.L.V. Prasad, M.J. Sastry, Mater. Chem. 15 (2005) 5115.

[8] S. Link, Z.L. Wang, M.A. El-Sayed, J. Phys. Chem. B 103 (1999) 3529.
[9] I. Srnova-Sloufova, F. Lednicky, A. Gemperle, J. Gemperlova, Langmuir 16 (2000) 9928.
[10] B. Rodriguez-Gonzalez, A. Burrows, M. Watanabe, C.J. Kiely, L. Liz-Marzan, J. Mater. Chem. 15 (2005) 1755.
[11] B. Jürgens, C. Kübel, C. Schulz, T. Nowitzki, V. Zielasek, J. Biener, M.M. Biener, A.V. Hamza, M. Bäumer, Gold Bull. 40 (2) (2007) 142.
[12] M. Haruta, Catal. Today 36 (1997) 153–166.
[13] V. Zielasek, B. Jergens, C. Schulz, J. Biener, M. Biener, A.V. Hamza, M. Bumer, Angew. Chem. Int. Ed. 45 (2006) 8241.
[14] D. Ferrer, D.A. Blom, L.F. Allard, S. Mejia, E. Perez-Tijerina, M. Jose-Yacaman, J. Mater. Chem. 18 (2008) 2442.
[15] H. Yoshida, C. Murata, T. Hattori, Chem. Commun. (1999) 1551.
[16] Y. Sun, B.T. Mayers, Y. Xia, Nano Lett. 2 (2002) 481.
[17] Y. Sun, B.T. Mayers, Y. Xia, Adv. Mater. 15 (2003) 641.
[18] J. Chen, B. Weily, Z.-Y. Li, D. Campbell, F. Saeki, H. Cang, L. Au, J. Lee, X. Li, Y. Xia, Adv. Mater. 17 (2005) 2255.
[19] Y. Yin, R.M. Rioux, C.K. Erdonmez, S. Hughes, G.A. Somorjai, A.P. Alivisatos, Science (2004) 711.
[20] D. Cheng, H. Xia, H.S.O. Chan, Nanotechnology 17 (2006) 1661.
[21] P.C. Lee, D.J. Meisel, Phys. Chem. 86 (1982) 3391.
[22] O.J. Scherzer, Appl. Phys. 20 (1949) 20.
[23] M. Jose-Yacaman, M.A. Borja, Catal. Rev. Sci. Eng. 34 (1992) 55.
[24] J.R. Davies (Ed.), Metals Handbook, ASM International, Materials Park, OH, 1998.